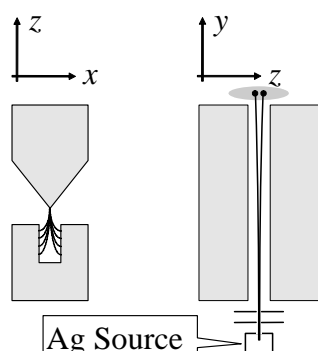


## 5 Paramagnetic Electron Resonance

By splitting the electron ground state in a strong external magnetic field, we get Zeeman resonances in the gigahertz range of the electromagnetic spectrum. The observation of these spectra is the basis of *electron paramagnetic resonance* (EPR) spectroscopy, which is also known as *electron spin resonance* (ESR). When Jewgeni Sawoiski first observed in 1944 electron spin resonance absorption in a copper(II) chloride dihydrate sample submerged in a 4.76 mT field at 133 MHz, electron paramagnetism had already been known for a long time. Otto Stern and Werner Gerlach had already demonstrated it in their famous experiment of 1921: a collimated beam of silver atoms, which are in the ground state  $^2S_{1/2}$  at room temperature (one 5s electron, the other shells are full or empty), passes parallel to the edge of the wedge-shaped pole shoe of an electromagnet, so that the magnetic field and its gradient are aligned parallel ( $z$ -axis). The atomic beam travels perpendicular to this direction. A homogenous magnetic field only affects the orientation of microscopic magnetic moments  $\mu$ , see chapter 4.1. The inhomogeneous magnetic field, however, applies a force in the  $z$  direction

$$\mathbf{F} = \mu_z \frac{dB}{dz} \text{ where } \mu_z = \frac{\mu \cdot \mathbf{B}}{B} \quad (5.01)$$

which diverts the atomic beam in this direction. From equ.(5.01), we get maximal deflection with opposite sign for microscopic magnetic moments in the  $z$  and  $-z$ -directions.



**Fig. 5.1** Stern-Gerlach Experiment. The cross section of the magnet, and the beam of silver atoms coming from the gas reservoir. The beam is collimated by masks and split in the inhomogeneous magnetic field. The detector was a cooled glass plate to which the silver atoms stuck. The spots were seen after chemical development.

According to classical laws, we should observe deflection in the direction of the gradient of the magnetic field for random orientations of  $\mu$  (except for perpendicular orientation of the dipole to the external field). In applying the inhomogeneous magnetic field, the cross section of the atomic beam was not even approximately continuous. Two spots instead of one were seen along the  $z$  axis. Two conclusions could be drawn from the experiment:

- 1) the existence of the magnetic moment of the electrons (whose connection to the spin of the electrons was first made in 1925 by Samuel Abraham Goudsmit and George Eugene Uhlenbeck), and
- 2) the proof of two preferred directions of the magnetic moment, which were later shown in quantum mechanics to be the magnetic quantization of the electron spins in an external field.

The Stern-Gerlach experiment was a major influence in the development of modern physics. It created a basis for the high frequency spectroscopic procedure used in the study of paramagnetic substances. In 1938, Isidor Isaak Rabi developed molecular beam resonance. EPR and NMR followed. NMR, treated in the previous chapter, is based on nuclear paramagnetism, and EPR is based on electron paramagnetism.

## 5.1 Electron Paramagnetism

A material is called paramagnetic, if it has no macroscopic magnetic moment in the absence of an external magnetic field, but in a magnetic field has one which points in the direction of the field. This can be understood by imagining that the stochastically oriented microscopic magnetic dipole moments are aligned by the external field. Thus, for the occurrence of electron paramagnetism, an atomic, ionic, or molecular magnetic moment is necessary. The existence of such a magnetic moment is the same as the existence of non-filled electron shells or the existence of unpaired electrons. Paired electrons have the same quantum numbers  $n$ ,  $\ell$ ,  $m$ , but opposite spin quantum numbers  $s = +\frac{1}{2}$  and  $s = -\frac{1}{2}$ . In atoms or molecules with only saturated electron shells, all electrons are paired, i.e. the resulting orbit and spin moments are zero. Nevertheless, such particles can often be examined with EPR if they are put in a paramagnetic ground state (e.g. creation of free radicals or triplet states) by, for example, irradiation.

EPR experiments concentrate on the following substances:

- a) Free radicals in solid bodies, liquids, or gases, which, according to definition, are an atom, molecule, or ion with an unpaired electron, e.g.  $\text{CH}_3$ . (The types mentioned later are excluded from the definition of a free radical.)
- b) The ions of the transition metals, belonging to the groups 3d, 4d, 5d, 4f and 5f of the periodic table. These include more than half of the elements of the known periodic table. The palette of various positive and negative ions contains up to 7 unpaired electrons.

In comparatively few experiments, EPR is also used to study the following substances:

- c) Solid bodies with defects. The most popular local point imperfection is the F-center which causes color effects. It is caused by an electron in an anion defect.
- d) Ions with a non bonding  $s$  electron (localized  $^2S_{\frac{1}{2}}$  state), e.g.  $\text{Ga}^{2+}$ .
- e) Systems with more than one unpaired electron except for those of point b). These include on the one hand systems in the triplet state, in which a strong interaction between the two unpaired electrons usually appears in an excited state, e.g. irradiated naphthalene. Bi-radicals, which show a weak interaction between the unpaired electrons and are therefore acting like two weakly interacting free radicals.
- f) Atom with non-filled electron shells, e.g. atomic hydrogen or atomic nitrogen and molecules with unpaired electrons, e.g. NO.
- g) Metals and semiconductors, which have unpaired electrons in their conduction bands.

It cannot, however, be expected that EPR experiments can be conducted on all the above substances in every case. A significant difference between NMR and EPR is just that: a strong influence of the surroundings on the orbital motion and through  $L$ - $S$ -coupling on the electron spins occurs in condensed material as a result of the strong coupling of the orbital magnetism to the surroundings. Thus the gyromagnetic ratio strongly depends on the environment of the paramagnetic ion. This is not true in NMR, where the resonance position only has a relatively weak dependency on interactions.

## 5.2 The $g$ -Factor and the Zeeman Splitting of Optical Spectra

In EPR, the most important parameter for the description of the spin system is the  $g$  factor. Before we define it, we will first briefly turn to orbital and spin magnetism, in which we will go from a classical to a quantum mechanical description.

An electron orbiting at radius  $r$  with the angular frequency  $\omega$  creates a current  $I = -e\omega/2\pi$  where the magnitude of the elementary charge  $e = 1,602 \times 10^{-19}$  C. In general, the magnetic moment of a current  $I$ , which encloses the surface  $A$ , is  $\boldsymbol{\mu} = IA$ . With  $A = r^2\pi$ ,  $\boldsymbol{\mu} = -1/2 e \omega r^2$ . With the angular momentum  $L = m_e r^2 \omega$  (electron mass  $m_e = 9,109 \times 10^{-31}$  kg), we get an orbital magnetism which depends on the angular momentum  $L$ :

$$\boldsymbol{\mu}_L = -\frac{e}{2m_e} \mathbf{L}. \quad (5.02)$$

For spin magnetism, we assume a rotating sphere of mass  $m_e$  and charge  $-e$  (the axis of rotation goes through the center of mass). We divide this sphere into infinitesimal volume elements, in which the ratio of segment charge through segment mass is independent of segment size. We then perform for each segment the same procedure that we used for an electron in a circular orbit and add all their contributions to the dipole moment. We get a magnetic moment dependent on the electron spin  $S$ , analogous to equ.(5.02):

$$\boldsymbol{\mu}_S = -\frac{e}{2m_e} \mathbf{S}, \quad (5.03)$$

in which  $S$  is the spin of the electron.

In analogy to NMR, see equations (4.01) to (4.03), because of the quantization of the angular momentum, we need the orbital angular momentum quantum number  $\ell$  and the spin quantum number  $s$  for the magnitude.

$$|\mathbf{L}| = \hbar\sqrt{\ell(\ell+1)} \quad \text{and} \quad |\mathbf{S}| = \hbar\sqrt{s(s+1)}. \quad (5.04)$$

The components in the direction of the external magnetic field in the  $z$ -direction are

$$L_z = \ell_z \hbar \equiv m_\ell \hbar \equiv m \hbar \quad \text{and} \quad S_z = m_s \hbar \equiv s \hbar. \quad (5.05)$$

There are  $2\ell+1$  magnetic quantum numbers for the orbital magnetism

$$m_\ell \equiv m = -\ell, -\ell+1, \dots, \ell-1, \ell \quad (5.06)$$

and only two magnetic quantum numbers for electron spin magnetism

$$m_s \equiv s = -1/2, +1/2, \quad (5.07)$$

in which the use of  $s$  in both the electron spin quantum  $+1/2$  and its magnetic quantum numbers  $\pm 1/2$  could lead to confusion.

If we consider the  $z$ -component of the magnetic moment in equ.(5.02) and use  $\hbar$ , which is the smallest non-zero value of the angular momentum  $L_z$  from equ.(5.06), we get the Bohr magneton as the elementary unit of magnetic orbital momentum in an external magnetic field.

$$\mu_B = -\frac{e}{2m_e} \hbar = 9,274 \cdot 10^{-24} \frac{\text{Jm}^2}{\text{Vs}}. \quad (5.08)$$

Based on the Bohr magneton, we will now introduce the  $g$  factor for an arbitrary magnetic quantum number  $m$  as:

$$|\boldsymbol{\mu}| = g\mu_B \sqrt{m(m+1)}. \quad (5.09)$$

In the following, we will use small letters for individual electrons and capital letters for multiple electrons. It follows directly from the comparison of equ.(5.09) with equ.(5.02) and equ.(5.04) that  $g_L = 1$  for orbital magnetism. This has been experimentally demonstrated with an accuracy of  $10^{-4}$ . Equations (5.03), (5.04) and (5.09) give us a  $g$ -factor that does not coincide with the experimental results for a free electron. If we use  $\frac{1}{2}\hbar$  for the electron spin  $S$  in equ.(5.06) and (5.07), we already have a discrepancy with the experimental fact that the intrinsic magnetic moment of the electron is a whole Bohr magneton, thus approximately the same as the one belonging to the orbital angular momentum quantum number  $\ell = 1$ .

Apparently the classical calculation, so successful in the case of orbital magnetism, fails to yield the correct results when applied to spin magnetism. This failure of the classical model is called the magnetic anomaly of the free electron. The correct theory was discovered by Paul Adrien Maurice Dirac in 1928 with his relativistic quantum mechanical description of the electron. The  $g$ -factor of the free electron is  $g_e = 2,002319304386(20)$ .

As mentioned at the beginning of the fourth chapter, magnetic resonance is related to the Zeeman effect, that is, on transitions between states that come into being through splitting in a magnetic field (usually the ground state). We will briefly explain what is meant by the normal and anomalous Zeeman effect in optical spectroscopy. The normal Zeeman effect appears in singlet states in which the total spin  $S = 0$ . It holds that  $J = L$ , all states are split  $2L+1$  times, and the distance between neighboring levels only depends on the external magnetic field. The selection rule for the change in the magnetic quantum number  $M$  in a transition is  $\Delta M = 0, \pm 1$ . From that we get three lines in optical transitions with  $\Delta L = 1$ , the normal Zeeman triplet. The splitting known for historical reasons as the anomalous Zeeman effect refers to the splitting of non singlet atoms. The Russel Saunders coupling is used for the addition of total orbital angular momentum and total spin:  $\mathbf{J} = \mathbf{L} + \mathbf{S}$ . The magnetic moments  $\boldsymbol{\mu}_L$  and  $\boldsymbol{\mu}_S$  point in the direction of  $\mathbf{L}$  and  $\mathbf{S}$ , according to equations (5.02) and (5.03). Because of the different values of  $g_L$  and  $g_e$ ,  $\boldsymbol{\mu}_J$  is no longer parallel  $\mathbf{J}$ , see Fig. 5.2.

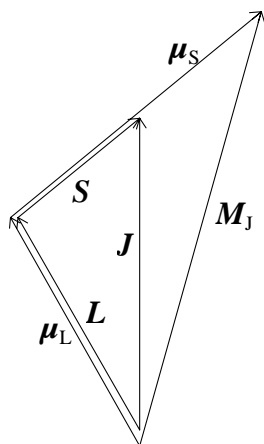


**Fig. 5.2** Vector diagram for the anomalous Zeeman effect. Due to  $L$ - $S$ -coupling,  $\mathbf{J} = \mathbf{L} + \mathbf{S}$ . The magnetic moments  $\boldsymbol{\mu}_L$  and  $\boldsymbol{\mu}_S$  are parallel to their angular momenta, and add to  $\mathbf{M}_J$ , which is not parallel to  $\mathbf{J}$ . The quantity  $|\boldsymbol{\mu}_J|$  used in equations (5.10) to (5.13) is not the magnitude of  $\mathbf{M}_J$  but its projection onto the  $\mathbf{J}$ -axis.

From equ.(5.09) we get the magnitudes of the magnetic moments:

$$|\mu_L| = g_L \mu_B \sqrt{L(L+1)}, \quad |\mu_S| = g_e \mu_B \sqrt{S(S+1)}, \quad |\mu_J| = g_J \mu_B \sqrt{J(J+1)}. \quad (5.10)$$

The resulting total angular momentum  $\mathbf{J}$  is constant in time.  $\mathbf{L}$  and  $\mathbf{S}$  precess around  $\mathbf{J}$ , so that only the components of their magnetic moments parallel to  $\mathbf{J}$  have an effect. From this it follows that

$$|\mu_J| = g_L \mu_B \sqrt{L(L+1)} \cos(\mathbf{L}, \mathbf{J}) + g_e \mu_B \sqrt{S(S+1)} \cos(\mathbf{S}, \mathbf{J}). \quad (5.11)$$

With the aid of the cosine law, we get an angle between  $\mathbf{L}$  and  $\mathbf{S}$  and  $\mathbf{S}$  and  $\mathbf{J}$  of

$$\cos(\mathbf{L}, \mathbf{J}) = \frac{|\mathbf{L}|^2 + |\mathbf{J}|^2 - |\mathbf{S}|^2}{2|\mathbf{L}||\mathbf{J}|} \quad \text{and} \quad \cos(\mathbf{S}, \mathbf{J}) = \frac{|\mathbf{S}|^2 + |\mathbf{J}|^2 - |\mathbf{L}|^2}{2|\mathbf{S}||\mathbf{J}|}. \quad (5.12)$$

With  $|\mathbf{L}| = \hbar \sqrt{L(L+1)}$ , see equ.(5.04) and the corresponding equations for  $\mathbf{S}$  and  $\mathbf{J}$  we get

$$|\mu_J| = \mu_B \frac{J(J+1)(g_e + g_L) + \{S(S+1) - L(L+1)\}(g_e - g_L)}{2\sqrt{J(J+1)}}. \quad (5.13)$$

If we connect equ.(5.11) with the lower line in equ.(5.10) and also set  $2g_L = g_e = 2$ , we get the factor named after Alfred Landé:

$$g_J = \frac{3J(J+1) + S(S+1) - L(L+1)}{2J(J+1)}, \quad (5.14)$$

He derived the factor using Bohr-Sommerfeld quantum mechanics and therefore used  $J^2$  instead of  $J(J+1)$  etc.. The  $g$  factor for the anomalous Zeeman effect is  $g_J$ . If strong magnetic fields disturb the  $\mathbf{L}$ - $\mathbf{S}$  coupling,  $\mathbf{L}$  and  $\mathbf{S}$  precess directly around the external magnetic field. As a consequence of this effect named after Friedrich Paschen and Ernst Back, the simple splitting associated with the normal Zeeman effect are again observed in optical transitions.

With that we return to EPR. In pure spin magnetism we expect  $g_e = 2,023$ , and this is truly observed in free radicals with an error of less than 10 %. In the transition metallic ions, the  $g$  factor can be negative in some cases, and can reach positive values of  $g \approx 4$ . In chapter 5.4 we will return to this in connection with the effective Hamiltonian.

### 5.3 Energy Splitting of the Ground State

We will now consider a special example, the  $\text{Cr}^{3+}$  ion, in which the shells 1s, 2s, 2p, 3s and 3p are fully occupied, but the shell 3d only has three electrons (5 in a neutral atom) and 4s is the first empty shell (1 electron in the neutral atom). Figure 5.3 shows a schematic representation of the splitting of the ground state. For the sake of simplicity, the figure does not consider two physical realities: the splitting in the electric field of neighboring ions (ligands) is orders of magnitude greater than that in the  $B_0$  field, and in the crossing of the levels with increasing  $B_0$ , level repulsion is not considered.

In the ground state of a non interacting ion, we have from the Hund rule  $L = 3$ ,  $S = 3/2$  and  $J = 3/2$ . The term symbol is  $^4F_{3/2}$ . The orbital angular momentum has 7 fold degeneracy, the spin 4 fold. In other words: the seven possibilities for  $L$  and four possibilities for  $S$  have the same energy. If the d electrons interact with the electric field of the ions in the vicinity (or with the crystal field), the ground state  $^4F_{3/2}$  is split. The orbitals of the d electrons are arranged in the symmetry types of point groups (irreducible representations, see chapter 3), which describe the symmetry of the Ligand field. In octahedral symmetry, this is the cubic point group  $O_h$ , in which the d electrons can occupy the orbitals  $A_{2g}$ ,  $T_{2g}$  and  $T_{1g}$ , which, compared to the free ion, results in a reduction or increase in energy.

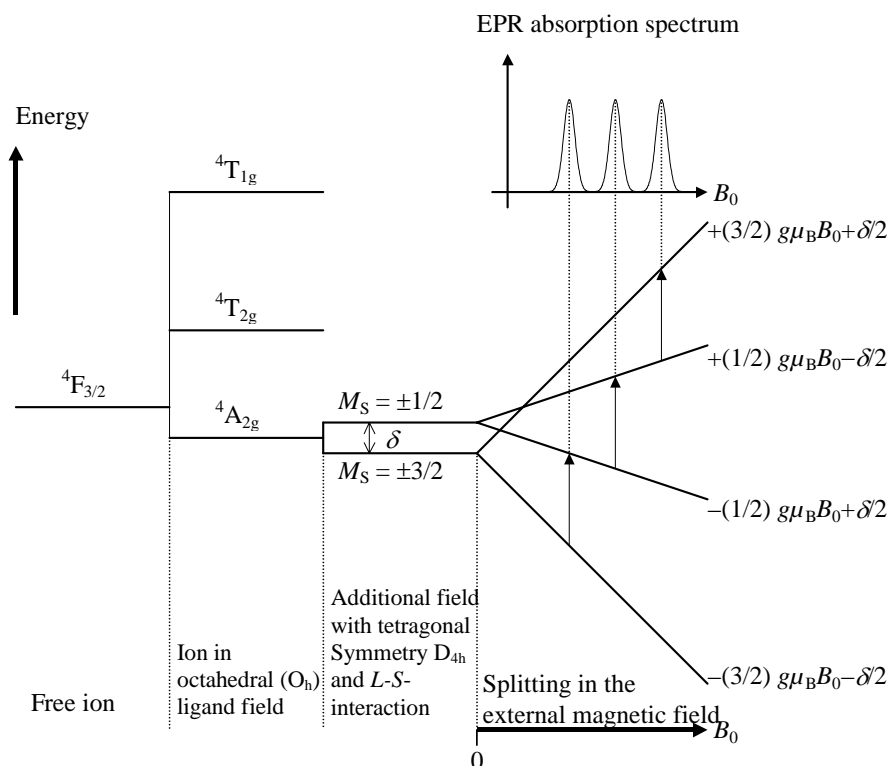


**Fig. 5.3** Splitting of the  $Cr^{3+}$ -ground state of the ion in a cation defect, e.g. in  $AlCl_3 \cdot 6H_2O$ .

For the  $Cr^{3+}$  ion in a ligand field with octahedral symmetry, the lowest level  $A_{2g}$  has no further orbital degeneracy, and  $M_L = 0$ . Therefore, we expect that  $J = S$  and  $g = 2,0023$ . (For  $Cr^{3+}$  in aluminum defects in an  $AlCl_3 \cdot 6H_2O$ -single crystal, experimental measurements show that  $g = 1,977$ .) If, however, there is an additional weak field with lower symmetry, e.g. axial symmetry, this influence together with a quadratic interaction relative to the electron spins leads to further splitting of the  $^4A_{2g}$  levels ( $^4$  refers to the spin degeneracy,  $A_{2g}$  to the symmetry group). This so-called zero field splitting creates two doubly degenerate states with  $M_J = \pm 1/2$  and  $M_J = \pm 3/2$  and energy difference  $\delta$ . The spin degeneracy is removed by the application of an external magnetic field. The energy separation is  $\Delta E = M_S g_S \mu_B B_z$ . Without zero field splitting, the energy difference for every two electron transitions with  $\Delta M_S = \pm 1$  would be the same, i.e. there would only be one line in the spectrum when taking into account the selection rule  $\Delta M_S = \pm 1$ . When  $\delta \neq 0$  we get the fine structure of the EPR spectrum (see the insert at the upper right of diag.3.5). It can be observed for  $S > 1/2$  if the ligand field symmetry differs from a pure cubic symmetry (primitive cubic, tetrahedral, or octahedral), and  $\delta < g_S \mu_B B_z$ , i.e. the energy of the zero field splitting is smaller than the Zeeman energy.

The splitting becomes anisotropic for zero field splitting smaller than the Zeeman energy and the resonant position depends on the orientation of the ligand field in the external magnetic field. This causes broadening of the resonance line as a result of the *powder pattern*. This pattern appears in non-crystalline solids with so many particles that all orientations of a principal axis system appear with equal probability. In single crystals, the spectra are dependent on the orientation. Figure 5.4 shows such angle dependency (the data is taken from G. Emch, R. Lacroix, and Helv. Phys. Acta 33 (1960) 745). To measure the spectrum, the sample is connected in such a way that it can be rotated about an axis (if possible a principle axis of the crystal system).

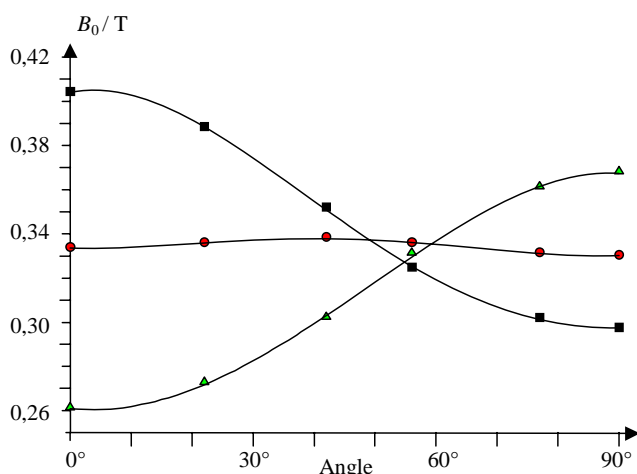


**Fig. 5.4** Angle dependency of the zero field splitting of EPR on the  $\text{Cr}^{3+}$  ion in a cation defect in an  $\text{AlCl}_3 \cdot 6\text{H}_2\text{O}$  single crystal. After Emch and Lacroix, reference in the text.

The most important splitting in an EPR spectrum is the hyper fine structure (HFS). The principal isotropic part of this interaction is caused by Fermi contact interaction of the charge density of s-orbitals at the nucleus with the nuclear spin. It was calculated by Enrico Fermi with good correlation to experiment. (p and d-orbitals have no charge density in the nucleus, see chapter 3.1.1). The christening as hyper fine interaction came from the analogy to splitting caused by electron-nuclear interactions in atomic spectra. An anisotropic hyper fine structure, only observable in solid state spectra, results from the interaction of the nuclear spin with a non-spherical electron orbital, e.g. a p-electron. It is analogous to dipolar splitting in NMR. Hyper fine splitting can be explained by a local field that creates the nuclear spin at the location of the electron. The EPR line is split into a doublet when  $I = 1/2$  with  $m_I = \pm 1/2$ :

$$B_{\text{Local}} = B_0 + a m_I. \quad (5.15)$$

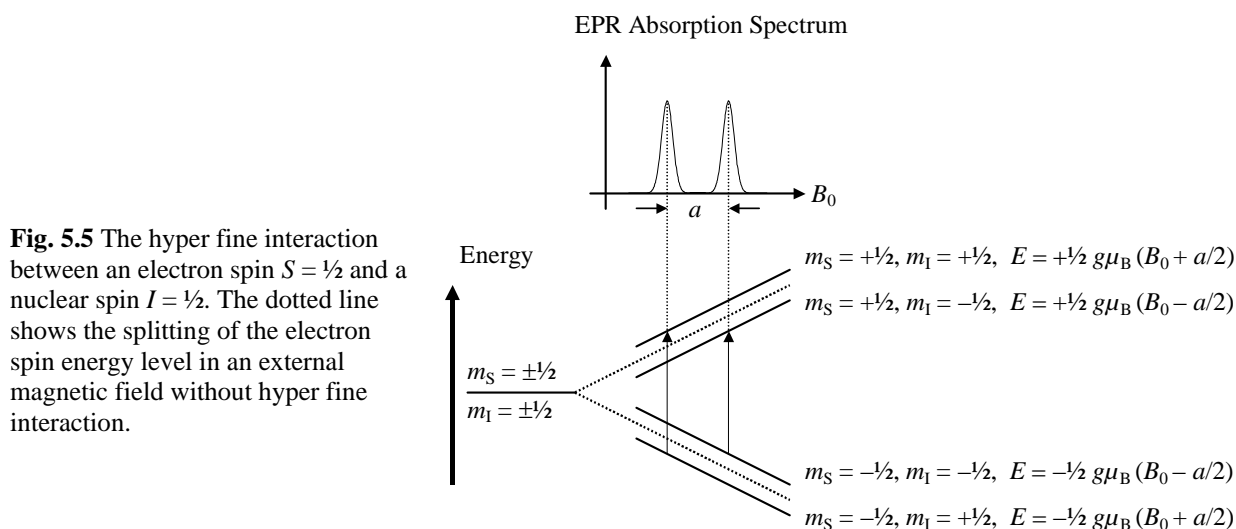


**Fig. 5.5** The hyper fine interaction between an electron spin  $S = 1/2$  and a nuclear spin  $I = 1/2$ . The dotted line shows the splitting of the electron spin energy level in an external magnetic field without hyper fine interaction.

The hyper fine coupling constant  $a$  is written here in units of Tesla. It is also given in Hertz. The electron-nuclear interaction of the s-orbitals leads to isotropic coupling constants. The p-orbitals in solid bodies lead to anisotropic coupling constants, which are described by a tensor  $T$ . Coupling constants for some nuclei and orbitals localized at those nuclei:  $^1\text{H} \leftrightarrow 1s$ : 50 mT,  $^2\text{H} \leftrightarrow 1s$ : 8 mT,  $^{14}\text{N} \leftrightarrow 2s$ : 55 mT,  $^{14}\text{N} \leftrightarrow 2p$ : 5 mT,  $^{19}\text{F} \leftrightarrow 2s$ : 1720 mT,  $^{19}\text{F} \leftrightarrow 2p$ : 108 mT.

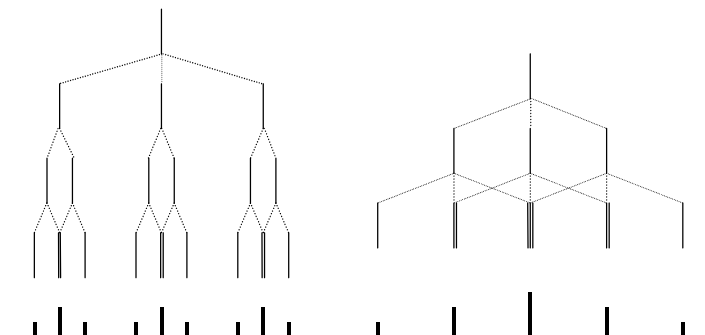


**Fig. 5.6** Hyper fine splitting (above) and intensity distributions (below) for two radicals. Left: radical composed of one nucleus with  $I = 1$  (z. B.  $^{14}\text{N}$ ) and two equivalent nuclei with  $I = \frac{1}{2}$  (e.g.  $^1\text{H}$ ). Right: radical composed of two equivalent nuclei with  $I = 1$  ( $^{14}\text{N}$  or  $^2\text{H}$ ).

For the nuclear spin  $I > \frac{1}{2}$  and multiple interacting nuclei, we get many splittings, see diag. 5.6. The splitting with  $n$  equivalent interacting spin  $\frac{1}{2}$  nuclei causes  $2n + 1$  equidistant lines, whose intensity relationships correspond to Pascal's triangle from diag. 4.13. In the Benzene radical anion,  $\text{C}_6\text{H}_6^-$ , the un-paired electron has equal probability of being found at all 6 carbon nuclei ( $^{12}\text{C}$  has no nuclear spin), which are each in the neighborhood of a spin  $\frac{1}{2}$  hydrogen nucleus. The EPR signal is therefore a sextet with intensity distribution 1:6:15:20:15:6:1, see diag. 4.13. The experimentally determined coupling constant is 0,375 mT. Evidence that the coupling constant corresponds to the density of the unpaired electrons in the atom with the interacting nuclear spin is found in the following: if we multiply the measured 0.375 mT by six (the number of nuclei over which the unpaired electron in the benzene radical anion is distributed), we get 2,25 mT. This is in good agreement with the value 2,3 mT for the  $\pi$  radical  $\text{CH}_3$ , in which the spin density of the unpaired  $\pi$  electron is located entirely at one carbon atom.

It is necessary here to add an explanation of why aromatic radicals display hyper fine splitting in liquids. Dipolar interactions are averaged out in a liquid, and  $\pi$  electrons have no charge density at the nucleus. The hyper fine splitting in aromatic radicals can, however, be explained by a polarization mechanism similar to  $J$  coupling in NMR, see chapter 4.5. The role of the anti-parallel electrons called for by Pauli's principle is taken by two  $\sigma$  electrons. One of these interacts with the  $^1\text{H}$  nuclear spin, the other with the unpaired  $\pi$  electron at the carbon atom.

We speak of a super hyper fine splitting in the EPR spectrum when the electron spin interacts with the nuclear spin of a neighboring atom.

#### 5.4 Spin Hamiltonian

For the spin Hamiltonian, we have to introduce a few basic physical terms. The time independent equation for the determination of the wave function  $\psi$  of a system, named after Erwin Schrödinger who found it in 1926 is

$$\mathcal{H}\psi = E\psi. \quad (5.16)$$

Although the energy on the right side of the equation can be thought of as a numerical factor (and an observable eigenvalue of the quantum mechanical system), the left side has an operator. The operator contains a procedure for mathematical operators that are to be applied to the wave function. For example, the procedure contained in the operator for a non-interacting particle of mass  $m$ , moving in the  $x$  direction through a potential  $V$ , is a double differentiation of the wave function  $\psi$ :

$$\mathcal{H} = -\frac{\hbar^2}{2m} \frac{d^2}{dx^2} + V. \quad (5.17)$$

This fundamental operator of quantum mechanics  $\mathcal{H}$  is named after William Rowan Hamilton, who put classical mechanics in a form which served as a basis for quantum mechanics 100 years later. The operator is a matrix, when related to spin variables. For the sake of simplicity, we will not use the hat often seen on operators, including the hamiltonian.

It is very unpleasant to describe a system with many degrees of freedom through a complete hamiltonian, whose energy eigenvalues determine the locations of all possible energy levels. Even for a simple atom whose nucleus is in the ground state, the contributions from the kinetic energy of the electrons, orbital energy, interaction energy between the electron spin and nuclear spin, nuclear Zeeman energy, and NMR interactions have to be taken into account.

The orders of magnitude of a few differences between corresponding eigenvalues are

Orbital energy	$> 10^4 \text{ cm}^{-1}$ ,
Energy splitting in ligand fields	$10^2 - 10^4 \text{ cm}^{-1}$ ,
Spin-orbit coupling for the atoms	B:10, C:28, F:271, Cl:440 und Br: 1842 $\text{cm}^{-1}$ ,
Electron-Zeeman transitions in X and Q-Band spectrometer	0,3 bzw. 1 $\text{cm}^{-1}$ ,
Spin-Spin coupling (Zero field splitting) for triplet ground state molecules	$\approx 1 \text{ cm}^{-1}$ ,
Electron spin – nuclear spin coupling (HFS)	$< 10^{-1} \text{ cm}^{-1}$ ,
Zeeman transitions of $^1\text{H}$ nuclear spins in a field $B_0 = 0,7 \text{ T}$	$10^{-3} \text{ cm}^{-1}$ .

The representation of energies in  $\text{cm}^{-1}$  (compare to Fig. 1.3) is often seen in EPR, even though the axes of the spectrum are often labeled with Tesla or the relative unit of the  $g$ -factor. The comparison of the above energies shows that the use of a complete hamiltonian would be unnecessary for the solution of the eigenvalue problem in EPR. A. Abragam and M.H.L. Pryce, Proc. Royal Soc. A205 (1951) 135, derived a spin hamiltonian which only takes the spin variables into account. It is constructed so that its eigenvalues correspond with the lowest level of the complete hamiltonian. With the Planck constant  $h$ , we get the spin hamiltonian for a Cartesian coordinate system  $x, y, z$  of the paramagnetic center and an axial crystal symmetry of the species (the symmetry axis  $z$  is the principal axis direction for the  $g$ ,  $D$ , and  $T$  tensor):

$$\mathcal{H} = g_{\parallel} \mu_B B_z S_z + g_{\perp} \mu_B (B_x S_x + B_y S_y) + D[S_z^2 - (1/3) S(S+1)] + hT_{\parallel} I_z S_z + hT_{\perp} (I_x S_x + I_y S_y). \quad (5.18)$$

Since we connected the Cartesian coordinate system to the crystal sample through equ.(5.18), no rule exists for the external magnetic field  $\mathbf{B}$  and the high frequency input field perpendicular to it. The orientation of  $\mathbf{B}$  can be arbitrarily set by rotating the sample. In equ.(5.18), an effective electron spin operator  $S$  can have an effect which is smaller than that shown by the multiplicity of the ground state. The first two terms on the right side of equ.(5.18) contain anisotropic effects of higher states from the spin-orbit coupling in addition to the scalar value  $g_e = 2,0023$ . The magnitude of these effects is different along an axis parallel  $g_{\parallel}$  and perpendicular  $g_{\perp}$  to the  $z$ -axis.  $D$  refers to the fine structure term which leads to zero field splitting. The tensor of the hyper fine coupling constant  $T$  can also assume different values for the electron-nuclear interaction parallel and perpendicular to the symmetry axis. The quadrupole and nuclear Zeeman terms belonging to the spin Hamiltonian have been left out of equ.(5.18) for the sake of simplicity.

If we only consider radicals in liquid samples, then the anisotropic parts are averaged out. We only need to deal with scalar values of  $g$  and  $T$ , and the fine structures disappear since  $D$  is now described by a zero-trace tensor.  $S = 1/2$ , and the isotropic  $g$ -factor differs from 2 by hardly more than 5%.

## 5.5 Experimental Detection of EPR

Although the first EPR experiment was done at 133 MHz, the frequencies currently in use range from 1 to 100 GHz. The most common EPR frequency is 9,5 GHz in the X-Band. In special applications, experiments are sometimes carried out in the S band (1,5-4 GHz) and C band (4-6 GHz). EPR spectrometers also operate in the K (11-36 GHz) and Q bands (36-46 GHz), which follow the X band (6-11 GHz). High-field EPR is conducted in the W band (55-100 GHz) at around 95 GHz and with a magnetic field of approx. 3,4 T. Attempts are being made with available super-conducting magnets at 15 T to move into the sub-millimeter range. As in NMR, the move to higher frequencies increases the spectral resolution.

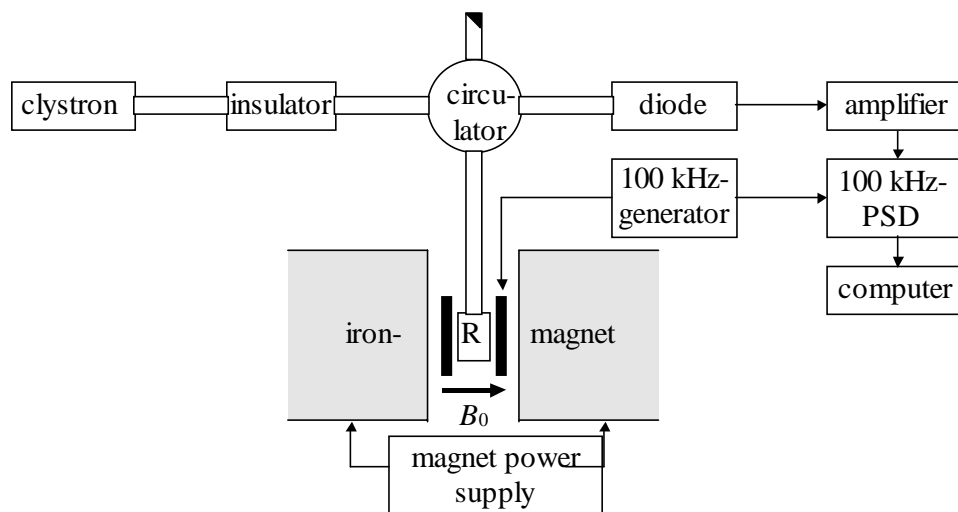


**Fig. 5.7** Basic construction of an X band EPR spectrometer with 100 kHz field modulation and phase sensitive detection (PSD). Between the klystron, resonator (R) and detector, a microwave frequency of about 10 GHz is transferred through square wave guides (cross-section 12,7×25,4 mm). Between the resonator and the two pole shoes of the magnet are modulation coils, which overlay a 100 kHz oscillating magnetic field onto the sample.

In the EPR laboratories there are still more continuous wave (cw) spectrometers than pulse spectrometers. The former work with the constant, continuously input microwave frequency of a klystron and the time-variable external magnetic field of an electromagnet, see Fig. 4.3. In the study of free radicals ( $g \approx 2$ ) at 9,5 GHz in the X band, magnetic induction of about 0,34 T is necessary. For the observation of a larger range of the  $g$  factor, magnets with an iron-core for a correspondingly larger field strength range are used. The spectrometer is composed of a frequency and power stabilized klystron sender, followed by an so-called insulator to decouple the sender. The attenuator which follows is not shown in Fig. 5.7. The circulator conducts the sender power to the sample, the power reflected to the detector, and the power reflected from the detector to the fourth arm, which serves as absorber. The resonator is located in the homogenous part of the magnetic field, contains the sample, and is constructed to heat the sample, and sometimes rotate single crystal samples. The detector is a microwave diode, which only rectifies the microwave frequency while leaving the modulation signal (100 kHz) untouched.

Continuous wave -EPR uses differential scanning (like broad-band cw-NMR, which is rarely seen today). The magnet power supply contains a setup to sweep a certain field range, so that a linearly time-varied external magnetic field  $B_0 = B_{\text{initial}} + \text{const.} \cdot t$  results. The external field is overlaid with an extra magnetic field with a frequency of, for example, 100 kHz, created by a pair of coils located between the pole shoes and the resonator. The amplitude of this extra field,  $B_{\text{Modulation}}$ , should be as large as possible for good signal-to-noise ratio, but smaller than the line width of the EPR signal to prevent false signals. The modulation frequency should also be less than the line width, since it causes side bands at a distance of the modulation frequency.

With that we get the complete time dependency of the external magnetic field:

$$B_0 = B_{\text{initial}} + \text{const.} \cdot t + B_{\text{modulation}} \cdot \sin(2\pi \nu_{\text{Modulation}} \cdot t). \quad (5.19)$$

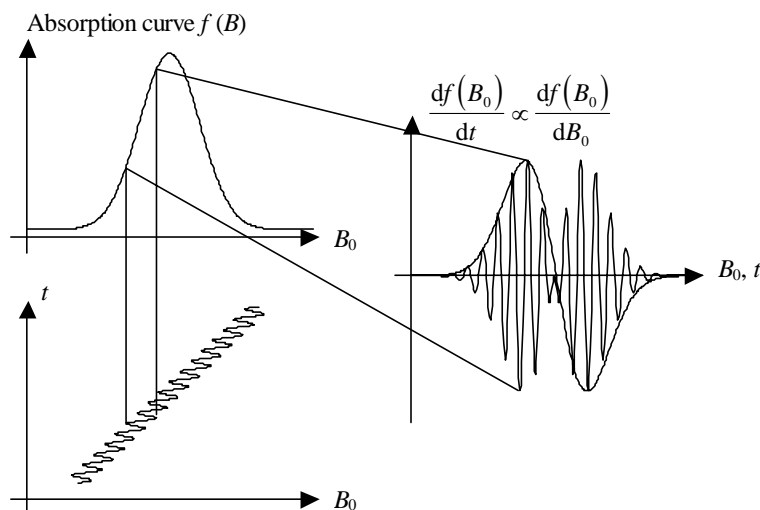


**Fig. 5.8** Differential scanning and phase sensitive detection.

Figure 5.8 shows how a Gaussian line defined as  $f(B) = \exp\{-(B - \alpha)/\beta\}$  is differentially scanned. The lower left of Fig. 5.8 shows the time dependency of the magnetic field from equ.(5.19). The field  $B_0$  scans the absorption signal like a characteristic curve. The dotted lines indicate the

passage of half a modulation period in the time domain. The steeper the slope (first derivative) of the absorption signal, the larger is the energy difference between two peaks of the modulation field. At the maximum of the absorption curve, this difference is zero. During passage through the maximum, the phase of the oscillating signal drawn lightly in the right part of Fig. 5.8 with the frequency  $\nu_{\text{modulation}}$  jumps by  $180^\circ$ . The oscillating signal is applied to the input of the phase sensitive detector (look in amplifier), and the phase sensitive detected signal is shown as a thick stretched-out line on the right side of Fig. 5.8.

To explain the phase sensitive detection, we again refer to Fig. 5.7. The 100 kHz signal coming from the detector is passed through a small-band amplifier and fed into the phase sensitive detector. This has another input, to which the 100 kHz reference frequency of the generator is applied, the same generator which drives the modulation coils. There is also a phase shifter not shown which assures that the signal and reference frequencies have the same (or opposite) phase. The phase sensitive detector is a multiplier followed by a low pass filter. The multiplier multiplies the signal function to the reference function (pure sine wave) and integrates with the help of the low-pass filter over an adjustable time period of a few seconds. In a mathematical sense, the operation of a phase sensitive detection is equivalent to the convolution of functions. From trigonometric identities we know that the product of two sinus function leads to two terms which contain the difference and sum of the arguments of the functions. The sum is suppressed by the low-pass filter and the phase difference plays an important role in the difference. The phase sensitive rectifier therefore creates the thick line from the thin one in Fig. 5.8. This curve corresponds exactly to the derivative of the absorption curve on the left side, if the modulation amplitude and time constant were sufficiently small to prevent signal falsification.

In all cw-EPR experiments, therefore, the differentially scanned signal is shown instead of the absorption curve. The signal shown corresponds to the first derivative of the absorption signal. (In Figs. 5.3 and 5.5, the absorption signals were shown for the sake of simplicity.) In a differentially scanned signal, structures are easier to recognize. There is, however, the significant disadvantage that the surface under the signal is not proportional to the concentration of the observed species. The most important advantage of the differential scanning of the signal is the improvement of the signal-to-noise ratio. With this procedure, the electronic bandwidth of the detection setup can be greatly reduced ( $< 1$  Hz), thanks to which the noise, which is proportional to the square root of the band width (see chapter 4.3) is reduced accordingly.

## 5.6 Pulse Measurement in Electron Spin Resonance

Pulse electron spin resonance spectrometers work in a fixed magnetic field, as in NMR. The highest achievable microwave power is applied in one or multiple pulses to rotate the macroscopic magnetization through the angle  $\pi/2$  or  $\pi$ , and plots the phase sensitive rectified signal as a function of time. It is advisable to review the previous lectures on NMR pulse measurements in chapter 4.6 to aid in the understanding of the EPR pulse measurement method dealt with here only briefly. Pulse EPR spectrometers are, for technical reasons, limited in their application to very wide lines (which are often seen in transition metals). Two conditions of high frequency spectroscopy, which in NMR are generally easy to fulfill, cause problems in EPR. First of all, the microwave field strength has to be so strong, that the  $\pi/2$  pulse of the entire spectrum to be observed is excited. A square pulse of length  $\tau$  has a bandwidth of around  $1/\tau$ . If the spectral width is 100 MHz, the pulse should not be longer than 10 ns. Achievable widths of  $\pi/2$  pulses range from 10-200 ns. The second problem is that the ring down of the pulse in the resonator and the overloading of the receiver electronics by the transmitter pulse that causes dead time in the receiver, in which no signal can be detected. This dead time should be shorter than the transversal relaxation time, which determines the free induction decay. A rough approximation of the transversal relaxation time from the reciprocal line width, see equ.(4.36), shows that this condition alone leads to a dead time of about 50 ns for a spectral width on the order of 10 MHz. This condition is less limiting, however, if we observe a Hahn-echo at time  $2\tau$  with a Hahn pulse train  $\pi/2, \tau, \pi$ , instead of the free induction decay (measurement begins immediately after the pulse) see chapter 4.6.

Despite the technical limitations, pulse electron spin resonance is applied in many areas. The simplest method, the Fourier transformation method (FT EPR) works with a single  $\pi/2$  pulse and plots the FID directly after the pulse. This method is particularly advantageous in the study of radicals, if optical radical creation is synchronized with the pulse experiment. Electron spin echoes are used in pulse EPR spectroscopy in many ways, similar to NMR, see chapter 4.6. The nuclear modulation effect in an EPR spectrum can be studied by varying the delay between the pulses of the echo pulse group and plotting the intensity of the echoes modulated by the electron-nuclear interaction (*echo envelope*) as a function of the pulse delay  $\tau$ . This process is called ESEEM (*Electron Spin Echo Envelope Modulation*) and can also be used in the study of relatively broad lines. The equation that describes the echo envelope contains cosine terms with arguments  $\omega_i \tau$ , where  $\omega_i$  corresponds to the nuclear resonance frequencies and their sums and differences. The effect only appears in solid bodies having an anisotropic electron-nuclear interaction. A few multi-dimensional methods of NMR have been applied to EPR. Such experiments are based on at least two independent variable times, in the simplest case the variable time  $\tau_1$  between two pulses and the variable time  $\tau_2$  for the scanning of the signal after the second pulse. Spectra are sequentially recorded with increasing pulse delay. The first Fourier transformation is performed relative to the scanning time  $\tau_2$  and gives an  $\omega_2$  representation, the second is performed relative to the pulse delay  $\tau_1$  and gives an  $\omega_1$  representation. As in nuclear resonance, the measurement of relaxation times with the cw method is hardly possible, and can only be achieved by pulse measurement.

## 5.7 ENDOR

**Electron Nuclear DOuble Resonance** detects nuclear spin transitions through the electron spin signal. An ENDOR spectrum has much higher resolution at greatly reduced detection sensitivity compared to a typical EPR spectrum. Another advantage is that the number of signals increases linearly with the number of nuclei thanks to the selection rules for nuclear spin transitions, in contrast to the quadratic increase in a normal EPR spectrum, see Fig. 5.6. For these reasons, ENDOR has become an important branch of EPR spectroscopy.

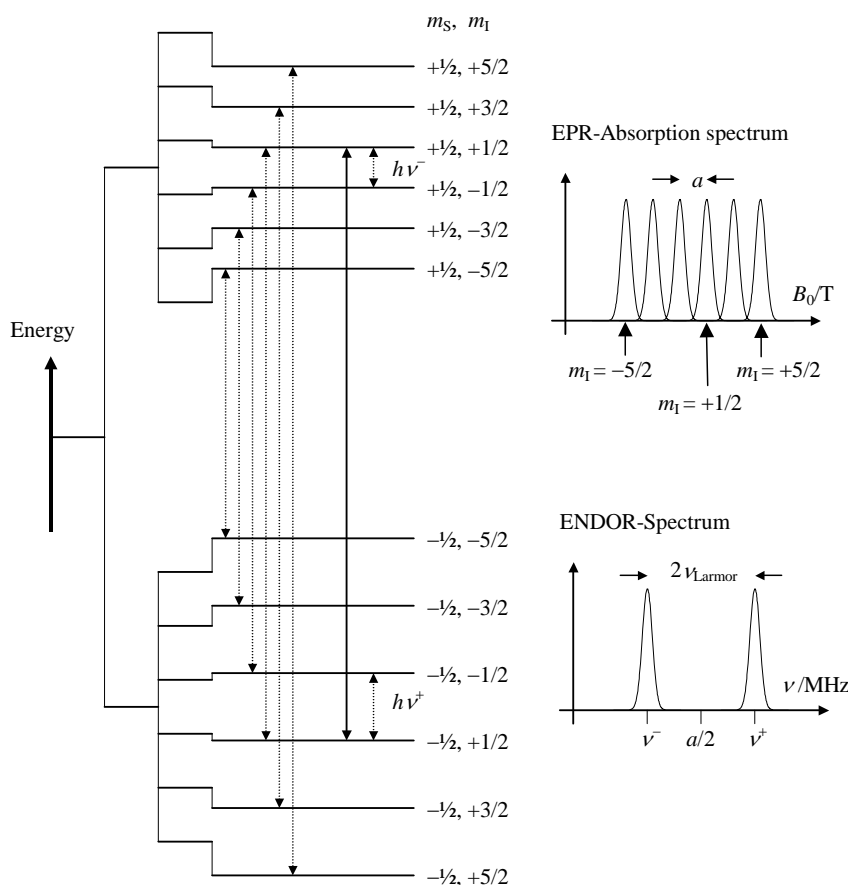


**Fig. 5.9** Energy levels, EPR-spectrum, and ENDOR spectrum of hyper fine interaction (or super hyper fine interaction) between an electron spin  $S = 1/2$  and a nuclear spin  $I = 5/2$ .

Figure 5.9 explains ENDOR detection in cw-EPR. The transitions between the

magnetic quantum numbers of the electron spin adhere to the selection rule  $\Delta m_S = \pm 1$ ,  $\Delta m_I = 0$ , the transitions between the nuclear spins obey the rule  $\Delta m_I = \pm 1$ ,  $\Delta m_S = 0$ . The electron ground state splits in an external magnetic field  $B_0$  corresponding to  $m_S = \pm 1/2$ .  $g$  refers to the electron  $g$ -factor and  $\mu_B$  is the Bohr magneton. Further splitting comes from the hyper fine interaction constant  $a$  proportional to  $m_I$ . An additional shift in the energy levels results from the nuclear Zeeman energy  $m_I \gamma \hbar B_0$ , in which  $\gamma$  is the gyromagnetic factor of the nucleus. In the figure, the nuclear Zeeman energy is smaller than the hyper fine interaction,  $E = m_S g \mu_B (B_0 + a m_I) - m_I \gamma \hbar B_0$ . The dotted transitions  $\Delta m_S = \pm 1$  show the EPR spectrum. The appearance of an ENDOR spectrum requires that one of the EPR transitions can be saturated by an strong microwave field. In Fig. 5.9, this transition is  $\Delta m_S = \pm 1$  and  $m_I = 1/2$ . Another high frequency field in the NMR frequency range is input with a frequency that increases in time (frequency sweep, similar to the otherwise common field sweep in EPR, see chapter 5.6). With a fixed magnetic field, the sweep interval of this high frequency in the MHz range covers the sum and difference of the Larmor frequency of the nuclear spin and half the frequency constant of the hyper fine interaction. If the high frequency now has the values  $\nu^+$  or  $\nu^-$ , then transitions can be induced which remove the balance of the occupation numbers of the levels caused by the saturation. The resulting difference in the occupation numbers causes microwave absorption, which can be measured with the EPR apparatus.

Pulse ENDOR spectroscopy does away with the irritating side-effects associated with the permanent saturation of the EPR transitions. It takes advantage of the fact that occupations are reversed by  $\pi$  pulses. On the one hand, an  $m_S = +\frac{1}{2}$  becomes  $m_S = -\frac{1}{2}$  after a resonant microwave  $\pi$  pulse, and on the other hand  $m_I = +\frac{1}{2}$  becomes  $m_I = -\frac{1}{2}$  after a high frequency  $\pi$  pulse. If an electron spin echo is created with microwave pulses, the echo can be removed by the simultaneous input of a resonant high frequency  $\pi$  pulse. If the high frequency is modified at constant magnetic field strength and constant microwave frequency, we get an pulse ENDOR spectrum.

## 5.8 Literature

- Abragam A. and Bleaney B.: EPR of Transition Ions, Clarendon, Oxford, 1970  
Atherton N.M.: Principles of Electron Spin Resonance, Ellis Horwood Ltd., Chichester, 1993  
Atkins P.W.: Physical Chemistry, Oxford University Press, Oxford Melbourne Tokyo, 1990  
Mabbs, F.E. and Collison D.: Electron Paramagnetic Resonance of Transition Metal Compounds, Elsevier, 1992, ISBN 0-444-89852-2  
Pake G.E. and Estle T.E.: The Physical Principles of EPR, Benjamin Cummings, Menlo Park, CA, 1970  
Pilbrow J.R.: Transition Ion Electron Paramagnetic Resonance, Clarendon, Oxford, 1990  
Schweiger A.: Puls-Elektronenspinresonanz-Spektroskopie, Angw. Chem. 103 (1991) 223  
Slichter C.P.: Principles of Magnetic Resonance, Springer, 1989  
Weil J.A., Wertz J.E. and Bolton J.R.: Electron Spin Resonance, Chapman and Hall, London, 1994, ISBN 0-471-57234-9